iJRASET
International Journal For Research in
Applied Science and Engineering Technology

INTERNATIONAL JOURNAL FOR RESEARCH
IN APPLIED SCIENCE & ENGINEERING TECHNOLOGY

Volume: 14 **Issue:** VII **Month of publication:** July 2026

DOI: https://doi.org/10.22214/ijraset.2026.84475

International Journal for Research in Applied Science & Engineering Technology (IJRASET)
ISSN: 2321-9653; IC Value: 45.98; SJ Impact Factor: 7.538
Volume 14 Issue VII July 2026- Available at www.ijraset.com

Simulation and Performance Analysis of Time-Modulated Array Beamforming

Chandanagiri Bhavani[1], Dr. M Madhavi Latha[2]
M.Tech in Systems and Signal Processing, Department of Electronics and Communication Engineering, JNTUH University College of Engineering, Science & Technology Hyderabad, Telangana, India

Abstract: Phased-array beamforming steers a beam electronically toward a Low Earth Orbit (LEO) satellite, but the phase shifter needed at every element makes the hardware costly, power-hungry, and difficult to scale for a compact Non-Terrestrial Network (NTN) user terminal. A conventional binary Time-Modulated Array (TMA) removes the phase shifter by switching each element ON/OFF in time, but its coarse two-state control caps achievable sidelobe level (SLL) and wastes radiated power in unwanted harmonics. This work develops a tri-state (+1, 0, −1) TMA for 5G New Radio (NR) NTN downlink terminals, in which each element is driven by an independent positive and negative pulse within a shared switching period. Closed-form harmonic coefficients are derived for the tri-state switching function and combined with the array steering vector to synthesise the first-harmonic radiation pattern. A Quadratic Programming Optimization (QPO) routine, warm-started with Chebyshev tapering, jointly minimises sidelobe level and half-power beamwidth (HPBW), while an Alternating Direction Method of Multipliers (ADMM) framework, realised as a Bartlett spatial-matched-filter coarse-to-fine search, adaptively tracks the satellite's direction of arrival (DoA). Simulated on a multi-element ULA driven by a realistic 5G NR OFDM waveform, the developed design reduces the sidelobe level from approximately −13 dB to −26 dB while improving output SINR and maintaining accurate beam tracking, with a beam pattern nearly indistinguishable from the ideal-DoA case, all at a considerably lower relative hardware cost than a fully phase-shifter-based array.
Keywords: Time-modulated array, tri-state switching, Non-Terrestrial Networks, beamforming, sidelobe suppression, quadratic programming, ADMM, direction-of-arrival estimation, 5G NR.

Table I. Key Notation

Symbol	Meaning
N	Number of ULA elements
T0, f0	Switching period and switching frequency (1/T0)
α_n	Normalised switching duration (duty cycle), element n
β_n	Switching instant, conventional binary TMA
β1,n, β2,n	Positive-/negative-pulse switching instants, tri-state
cm,n	mth-harmonic Fourier coefficient, element n
a(θ), θ	Steering vector; direction of arrival
d, λ, k	Element spacing, wavelength, wave number (2π/λ)
AFm(θ)	Array factor of the mth harmonic
SLL, HPBW	Sidelobe level, half-power beamwidth
J(α), w1, w2	QPO cost function and its weighting factors
z, λ, ρ	ADMM auxiliary variable, multiplier, penalty parameter

I. INTRODUCTION

Modern wireless services such as cloud computing, smart-city infrastructure, autonomous vehicles, remote healthcare, and large-scale IoT rely on a backbone that has grown more spectrally efficient with every cellular generation. Fifth-generation (5G) networks build enhanced mobile broadband, ultra-reliable low-latency communication, and massive machine-type communication on massive MIMO, millimetre-wave links, and beamforming, which concentrates radiated power along a chosen direction to govern signal quality, coverage, and interference control.

Terrestrial towers cannot economically reach mountains, deserts, oceans, and disaster zones, which is why 3GPP now folds Low Earth Orbit (LEO), Medium Earth Orbit, and Geostationary satellites into the 5G/6G roadmap as Non-Terrestrial Networks (NTNs). LEO is attractive for its low propagation delay and path loss, but its fast sky transit forces the ground terminal to continuously track a moving direction of arrival (DoA) while maintaining high gain, precise steering, and interference rejection in a compact, power-frugal package.

Conventional phased-array beamforming meets these demands electronically through a dedicated RF phase shifter at every element, but its complexity, power draw, and calibration effort all scale badly with array size a serious constraint for a portable NTN terminal. Consequently, low-complexity beamforming architectures are required for portable NTN user terminals operating under stringent power and hardware constraints. The Time-Modulated Array (TMA) instead replaces the phase shifter with a high-speed RF switch, trading continuous phase control for switching timing. A conventional binary TMA is inexpensive but switches each element only fully ON or OFF, a coarse excitation control that generates unwanted harmonic radiation and caps achievable sidelobe suppression. Because periodic switching is inherently a harmonic-generating process, a suitably designed switching sequence can also put the normally wasted higher-order harmonics to use as additional, largely independent beams from the same aperture a shared-aperture multibeam capability that neither a conventional phased array nor a digital beamformer offers without dedicated per-beam RF chains or ADCs.

Giving each element a third state driven positive (+1), OFF (0), or driven negative (−1) restores a meaningful degree of excitation control without reintroducing a phase shifter. This tri-state switching scheme, first proposed by Lema et al. [1], is the starting point for the present work, which reproduces and extends it with a complete signal-to-performance simulation pipeline built around a realistic 5G NR NTN downlink waveform, closed-form harmonic-coefficient derivations, a QPO stage for sidelobe suppression, and an ADMM-based adaptive tracking stage for a moving LEO DoA.

A. Contributions

Unlike existing TMA studies, which typically validate switching-based beamforming on an idealised narrowband tone and report pattern-level metrics in isolation, this work grounds every stage in an executable pipeline driven by a realistic 5G NR OFDM waveform and reports both pattern-level and link-level outcomes together. Specifically, this paper contributes:

1) A baseband-to-RF simulation pipeline built around a realistic 5G NR OFDM downlink waveform at an L-band NTN carrier frequency of 1.55 GHz;
2) Closed-form harmonic-coefficient and array-factor derivations for the tri-state switching function, distinguishing it from the conventional binary case;
3) A QPO-based sidelobe/beamwidth optimisation stage, warm-started with Chebyshev amplitude tapering, that pushes SLL from about −13 dB to about −26 dB;
4) An ADMM-based adaptive tracking framework, realised as a Bartlett spatial-matched-filter coarse-to-fine grid search, for continuous DoA tracking; and
5) A system-level evaluation spanning SLL, HPBW, gain, SINR, BER, and EVM, together with a relative hardware-cost and power-consumption comparison against conventional phased-array and digital beamforming.

Unlike previous TMA studies that mainly focus on radiation-pattern evaluation, this work integrates realistic 5G NR waveform generation, tri-state switching, QPO optimisation, adaptive beam tracking, and communication-level performance evaluation within a single simulation framework. The rest of the paper is organised as follows. Section II reviews the prior work this formulation builds on. Section III sets up the NTN signal and array models. Section IV derives the tri-state switching function, its harmonic coefficients, and the resulting array factor. Section V presents the QPO and ADMM-based optimisation stages. Section VI describes the simulation setup, Section VII reports the results, and Section VIII concludes with directions for future work.

II. LITERATURE REVIEW

Lema et al. [1] proposed a TMA beamforming framework for NTN user terminals that replaced RF phase shifters with high-speed RF switches and compared binary against tri-state switching across SLL, HPBW, gain, and hardware complexity, finding better sidelobe suppression and harmonic utilization at lower complexity and power; their paper also introduced the QPO and ADMM concepts extended here, while noting that further validation under practical conditions was still needed. Kummer et al. [2] established the underlying physics of time-modulated arrays, showing analytically that periodic switching generates ultra-low sidelobes together with harmonic sideband radiation the classical basis for the harmonic-coefficient derivations used throughout this paper. Balanis [3] and Van Trees [4] respectively provide the array-theory fundamentals (steering vectors, array factors, tapering) and the adaptive array-processing fundamentals (DoA estimation, spatial matched filtering) that the tri-state formulation and the adaptive DoA-tracking stage build on.

Boyd et al. [5] developed the Alternating Direction Method of Multipliers, combining augmented Lagrangian methods with dual decomposition for reliable convergence on large-scale constrained problems, motivating its use here for adaptive beam tracking. The 3GPP Release-17 specifications [6], [7] define the NR physical layer, waveform generation, and NTN-capable architecture that the simulated downlink signal follows. Azari et al. [8] survey this broader 5G-to-6G NTN evolution, situating the terminal-level beamforming problem tackled here within the wider NTN research landscape.

Taken together, this body of work explains why NTN beamforming is difficult phased arrays steer well but do not scale cheaply, while conventional TMAs are cheap but historically lose sidelobe performance and what tools exist for closing that gap. This paper differs from [1] by grounding every stage in an executable pipeline driven by a realistic OFDM waveform, by implementing a Bartlett-embedded coarse-to-fine grid search within an ADMM-style iteration for adaptive DoA tracking, and by reporting link-level metrics (BER, EVM) alongside pattern-level metrics.

III. SYSTEM MODEL

A. NTN Downlink Signal

The system operates on a realistic 5G NR NTN downlink signal rather than an idealised sinusoid, using a practical OFDM-based waveform representative of an L-band satellite scenario. L-band is attractive for satellite mobile communication owing to favourable propagation and low atmospheric attenuation; 3GPP NTN specifications place the L-band downlink at roughly 1.525–1.559 GHz, and a representative carrier of fc = 1.55 GHz is used here.

The complex baseband in-phase/quadrature waveform is up-converted to obtain the RF signal

$$s_{RF}(t) = Re\{ baseband\_signal(t) \cdot e^{j2\pi f_c t} \} \quad (1)$$

where baseband_signal(t) is the complex IQ waveform produced by the 5G NR waveform generator and Re{·} denotes the real part. The resulting waveform exhibits the noise-like, wideband envelope expected of a 10 MHz 5G NR NTN downlink, confirming realistic multi-subcarrier OFDM behaviour.

B. Array Received Signal and Steering Vector

Treating the RF signal as arriving at a Uniform Linear Array (ULA) from the LEO satellite direction, the down-converted received array signal is

$$x(t) = s(t) \cdot a(\theta) + n(t) \quad (2)$$

where x(t) is the received array vector, s(t) is the received baseband signal, a(θ) is the steering vector for DoA θ, and n(t) is additive white Gaussian noise. For an N-element ULA with inter-element spacing d = λ/2,

$$a(\theta) = [1, e^{jkd\, sin\theta}, e^{j2kd\, sin\theta}, \dots, e^{j(N-1)kd\, sin\theta}]^T \quad (3)$$

with k = 2π/λ the wave number. This steering vector underlies the array-factor synthesis, DoA estimation, and beam-steering evaluation used throughout the paper.

C. Conventional Binary Switching

In a conventional TMA, each element's excitation over one modulation period T0 follows the binary switching function

$$g_n(t) = \begin{cases} +1, & \beta_n T_0 \le t < (\beta_n + \alpha_n)T_0, \\ 0, & \text{otherwise.} \end{cases} \quad (4)$$

where α_n is the normalised switching duration (duty cycle) and β_n the normalised switching instant. Being periodic, $g_n(t)$ admits a Fourier-series expansion whose m^th harmonic coefficient, following the classical derivation of [2], reduces to

$$c_{m,n} = [sin(\pi m \alpha_n)/\pi m] \cdot e^{-j\pi m(2\beta_n + \alpha_n)} \quad (5)$$

This coefficient sets the amplitude and phase of each harmonic, but binary switching offers only one duty-cycle and one switching-instant parameter per element the coarse control responsible for the elevated sidelobes reported for conventional TMAs.

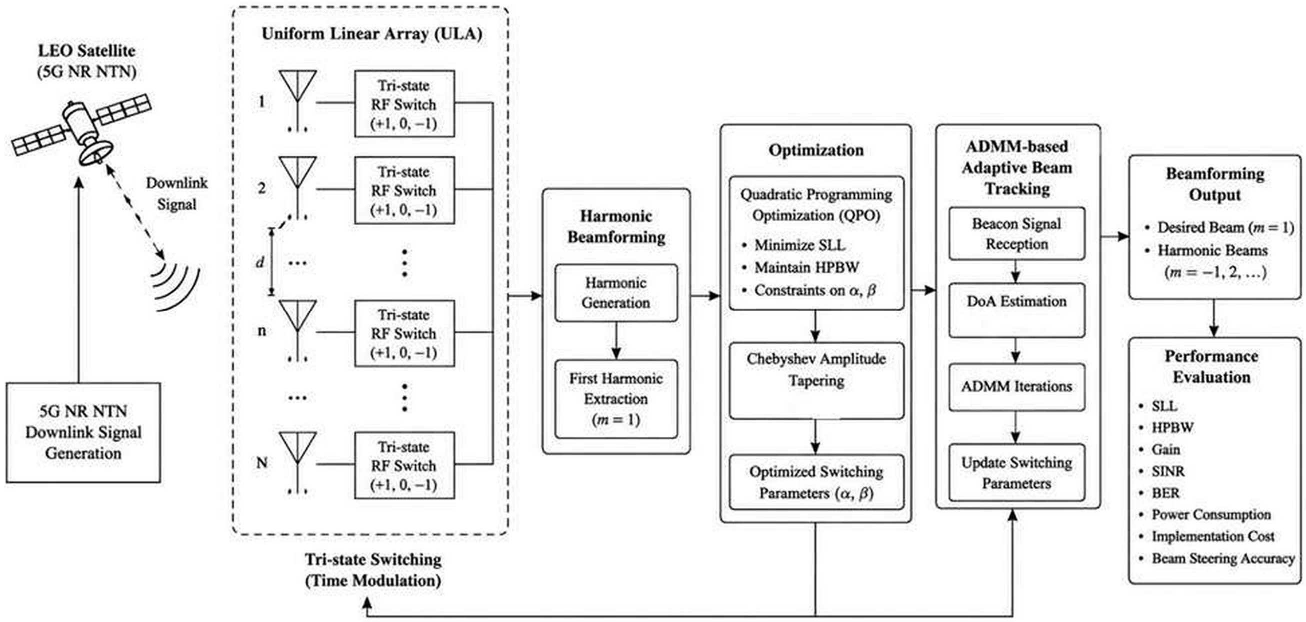

Fig. 1. Overall system architecture: 5G NR NTN downlink reception, per-element tri-state switching, harmonic and array-factor computation, QPO-based sidelobe optimisation, and ADMM-based adaptive DoA tracking.

IV. TRI-STATE TMA BEAMFORMING

Fig. 1 summarises the overall signal chain: a 5G NR NTN downlink signal is received at the ULA, each element's tri-state switch operates on the durations and instants set by the downstream optimisation stages, the harmonic coefficients and first-harmonic array factor are computed, QPO tunes the switching parameters (combined with Chebyshev tapering) for sidelobe suppression, and the ADMM-based Bartlett tracker keeps the resulting pattern locked onto the estimated DoA.

A. *Tri-State Switching Function*

The developed scheme excites each element with two independent pulses within a single period a positive-state pulse and a negative-state pulse leaving the element OFF otherwise:

$$g_n(t) = \begin{cases} +1, & \beta_{1,n}T_0 \le t < (\beta_{1,n} + \alpha_n)T_0, \\ -1, & \beta_{2,n}T_0 \le t < (\beta_{2,n} + \alpha_n)T_0, \\ 0, & \text{otherwise.} \end{cases} \quad (6)$$

where β1,n and β2,n are the switching instants of the positive and negative pulses respectively and α_n is again the normalised duty cycle, shared by both pulses. Unlike the binary case, this function carries two independently placed active intervals per period, giving each element independent control over positive and negative excitation.

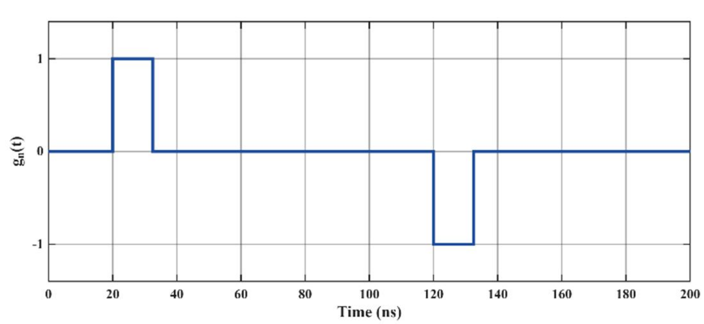

Fig. 2. Tri-state switching waveform: element state over one modulation period T0.

B. Harmonic Coefficient of the Tri-State Function

Integrating $g_n(t)$ over one period and evaluating the positive and negative intervals separately, then applying Euler's identity, gives the closed-form tri-state harmonic coefficient

$$c_{m,n} = [sin(\pi m\alpha_n)/\pi m] \cdot [e^{-j\pi m(2\beta_{1,n}+\alpha_n)} - e^{-j\pi m(2\beta_{2,n}+\alpha_n)}] \quad (7)$$

Compared with (5), this coefficient carries two independent exponential terms, one per polarity: the magnitude still depends on α_n, while β1,n and β2,n jointly set the relative phase between the positive and negative contributions. Setting β2,n = β1,n + α_n recovers the special case in which the negative pulse immediately follows the positive one, used as a baseline configuration before QPO searches the full (α_n, β1,n, β2,n) space.

Allowing β1,n and β2,n to vary independently is precisely what lets QPO shape the relative phase between positive and negative excitation per element the mechanism ultimately responsible for the sidelobe reduction reported in Section VII.

C. First-Harmonic Array Factor and Harmonic Diversity

Combining the harmonic coefficients with the array steering vector gives the radiation pattern of the m[th] harmonic for an N-element ULA,

$$AF_m(\theta) = \sum_{n=0}^{N-1} c_{m,n}\, e^{jknd\, sin\theta} \quad (8)$$

The first harmonic (m = 1) serves as the primary communication beam and is the harmonic optimised by QPO in Section V-A. Because different harmonic orders exhibit independent patterns, the same tri-state switching sequence generates additional, largely independent beams from higher harmonics a shared-aperture multibeam capability requiring no extra RF chains, examined quantitatively in Section VII-D.

V. OPTIMIZATION FRAMEWORK

A. Quadratic Programming Optimization (QPO)

Arbitrary switching-duration choices can leave sidelobe levels elevated even with the added tri-state degree of freedom. QPO searches for the duty-cycle vector α that minimises a blended cost function

$$J(\alpha) = w_1 \cdot SLL(\alpha) + w_2 \cdot HPBW(\alpha) \quad (9)$$

subject to $0.01 \le \alpha_n \le 0.49$ for every element n, a range that keeps the switching intervals physically realisable.

The optimisation loop (i) initialises α_n warm-started from a Chebyshev amplitude taper generated for a −25 dB design sidelobe level; (ii) computes the tri-state harmonic coefficients and first-harmonic array factor; (iii) evaluates SLL and HPBW from the resulting pattern; (iv) evaluates J(α); (v) updates α via the QPO solver; and (vi) repeats until convergence, storing the optimised switching parameters for beamforming. Because the unweighted sinc-based tri-state pattern cannot reach a −25 dB target through duty-cycle tuning alone, the amplitude taper from the Chebyshev warm start is carried through as the effective per-element weighting that QPO refines.

B. ADMM-Based Adaptive Beam Tracking

Because the satellite's DoA shifts continuously, a beamforming solution fixed at one direction cannot sustain maximum gain throughout the link. Adaptive tracking is posed as

$$min\, f(\alpha) + g(z) \;\; s.t.\; \alpha = z \quad (10)$$

where z is an auxiliary variable that splits the problem into simpler alternating subproblems, with augmented Lagrangian

$$L(\alpha, z, \lambda) = f(\alpha) + g(z) + \lambda^T(\alpha - z) + (\rho/2)||\alpha - z||^2 \quad (11)$$

$$\alpha^{k+1} = argmin_\alpha\, L(\alpha, z^k, \lambda^k);$$
$$z^{k+1} = argmin_z\, L(\alpha^{k+1}, z, \lambda^k);$$
$$\lambda^{k+1} = \lambda^k + \rho(\alpha^{k+1} - z^{k+1}) \quad (12)$$

The tracking loop then (i) receives the beacon signal from the satellite, (ii) estimates the DoA, (iii) updates α via the ADMM procedure, (iv) recomputes the harmonic coefficients and array factor, (v) evaluates steering error, and (vi) repeats until convergence before steering the beam to the estimated position.

The DoA estimate itself is obtained through a Bartlett spatial-matched-filter search evaluated on a coarse-to-fine angular grid (1° → 0.1° → 0.01°), embedded inside the primal/auxiliary/dual ADMM iteration, while retaining the ADMM-style iterative structure of (10)–(12).

VI. SIMULATION SETUP

The developed beamforming framework was evaluated through numerical simulations using signal-processing and constrained optimization techniques, covering 5G NR waveform generation, the QPO optimisation stage, and the ADMM-based tracking and harmonic-beamforming computations.

Table II lists the simulation parameters. Sidelobe level, half-power beamwidth, antenna gain, SINR, and BER/EVM are evaluated as defined in [1]–[4], with SINR computed for a six-beam independent-interferer scenario in which each interferer is generated as its own 5G NR waveform arriving from a distinct DoA.

Table II. Simulation Parameters

Parameter	Value
Carrier frequency, fc	1.55 GHz
Switching frequency, F0	5 MHz
Signal bandwidth	10 MHz
Waveform	5G NR OFDM
Antenna array	Uniform Linear Array
Number of elements, N	16
Inter-element spacing, d	λ/2
Optimisation algorithm	QPO
Adaptive tracking algorithm	ADMM-based (Bartlett search)
Harmonic used for pattern synthesis	First harmonic (m = 1)

VII. RESULTS AND DISCUSSION

Unless otherwise stated, all reported results correspond to the first harmonic (m = 1), which serves as the primary communication beam. The beamforming system was evaluated using radiation-pattern, communication, and hardware metrics. The tri-state design was compared against conventional single-pulse and uniform-duty switching to assess sidelobe suppression, beam steering accuracy, communication quality, and power efficiency across a common set of test conditions.

A. Sidelobe Suppression

Table III compares single-pulse switching, uniform-duty tri-state switching, and the tri-state + QPO design. Both baselines sit at about −13.15 dB SLL, short of the −25 dB target; the QPO design (warm-started with Chebyshev tapering) reaches −25.53 dB, at a cost of about 0.3 dB peak gain (13.63 dBi to 13.25 dBi) and a modest HPBW increase (6.77° to 8.00°), while output SINR improves from 8.32 dB to 22.16 dB under a six-interferer scenario.

Table III. Performance Comparison of Beamforming Approaches

Method	SLL (dB)	HPBW (°)	Gain (dBi)	SINR (dB)	Rel. HW Cost (norm.)
Single-pulse (baseline)	−13.15	6.77	13.63	8.32	~35
Tri-state, uniform duty	−13.15	6.77	13.63	14.34	~35
Tri-state + QPO (proposed)	−25.53	8.00	13.25	22.16	~45

This gain–sidelobe trade-off matches classical amplitude-tapering behaviour for array antennas [3]: pulling energy out of the sidelobes narrows the effective aperture illumination and costs a small amount of directivity, and a 0.3 dB cost for roughly 12 dB of sidelobe suppression is a favourable exchange. The hardware-cost column (Section VII-C) is included alongside the pattern metrics because the tapered design uses the same switch count as the untapered one only the DSP-level control and a modest cost increase differ.

The nearly 14 dB SINR improvement is the more consequential result for a satellite link budget: interference leakage through elevated sidelobes, rather than raw gain, is typically the limiting factor in a multi-beam or multi-satellite NTN scenario.

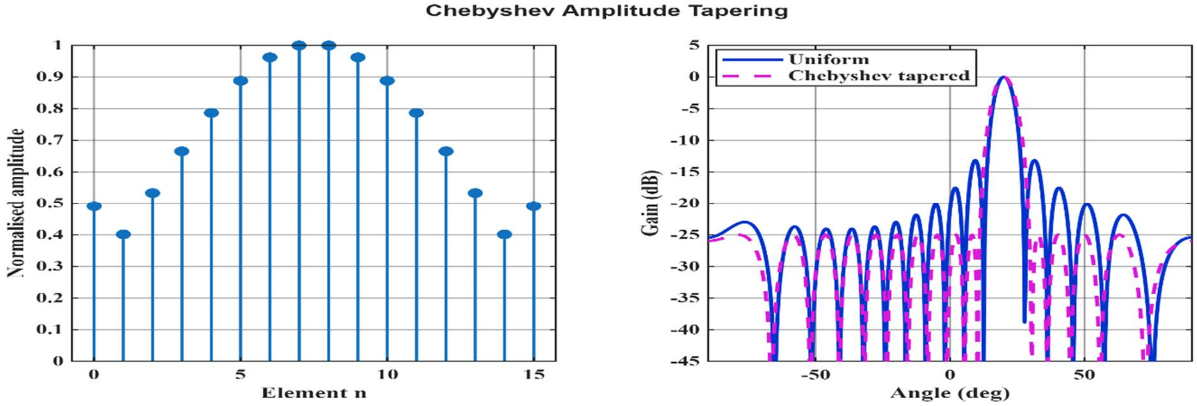

Fig. 3. Chebyshev amplitude taper coefficients across the array (left) and the corresponding beam pattern (right), used as the QPO warm start.

Fig. 3 shows the Chebyshev taper coefficients used to warm-start QPO (left) and the resulting beam pattern (right). The taper follows the expected bell-shaped profile, tapering the outer elements to roughly 0.40–0.49 of the peak amplitude at array centre, and holds sidelobes uniformly at about −25 dB, compared with about −13 dB for the untapered array immediately next to the mainlobe — the classical equi-ripple behaviour expected of a Dolph–Chebyshev design, confirming the taper generation works correctly ahead of being used as the QPO warm start.

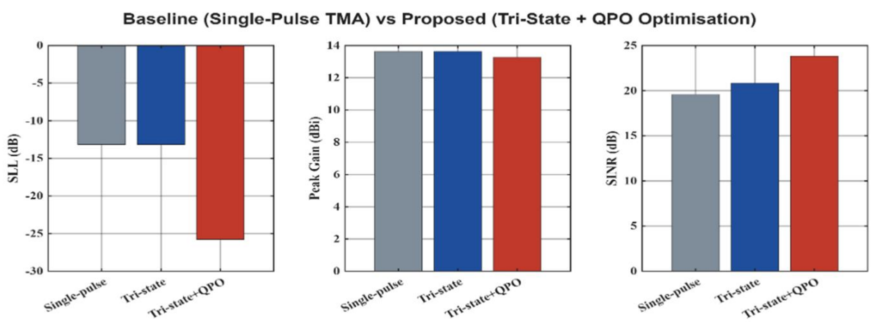

Fig. 4. SLL, HPBW, peak gain, and SINR across the three switching schemes of Table III.

Table IV examines the spread of the optimised duty cycles α_n across the 16 elements. In the uniform baseline every element shares $\alpha = 1/N = 0.0625$ by construction. Once QPO is allowed to vary α_n per element, the values spread from 0.1183 to 0.4224 with a standard deviation of 0.1039, and none of the optimised values sit at either constraint bound confirming genuinely interior, non-degenerate solutions rather than an artefact of the 0.01–0.49 constraint window.

Table IV. Spread of Optimised Duty Cycles α_n (16 Elements)

Method	min(α)	max(α)	std(α)
Uniform (baseline)	0.0625	0.0625	0.0000
QPO (proposed)	0.1183	0.4224	0.1039

B. DoA Tracking and Link-Level Performance

The ADMM tracking pattern is nearly indistinguishable from the tri-state baseline pattern computed with the true DoA, confirming that the coarse-to-fine grid search converges correctly even without perfect DoA knowledge, and that sidelobe suppression and DoA estimation operate independently of one another (Fig. 5).

International Journal for Research in Applied Science & Engineering Technology (IJRASET)
ISSN: 2321-9653; IC Value: 45.98; SJ Impact Factor: 7.538
Volume 14 Issue VII July 2026- Available at www.ijraset.com

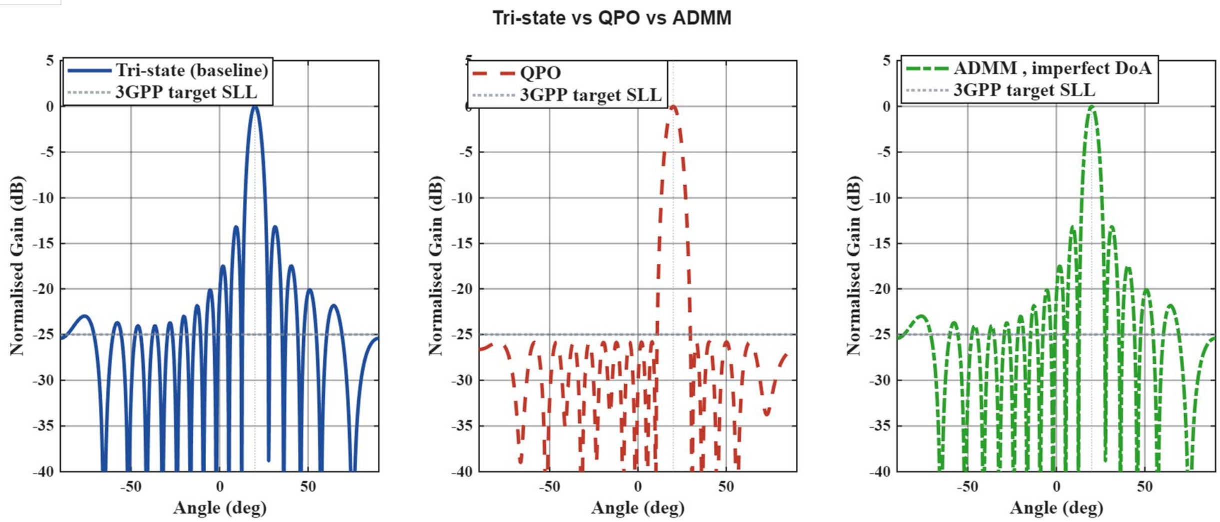

Fig. 5. Beam-pattern comparison of the tri-state baseline, the QPO-tapered design, and the ADMM-tracked pattern under an imperfect initial DoA, all steered to 20° against the 3GPP −25 dB SLL target. The ADMM panel confirms that Bartlett-based tracking converges the beam back onto the true DoA despite the imperfect starting estimate.

This carries through to link-level metrics. BER falls steadily with SNR for both 12- and 16-element arrays: as SNR increases, the desired signal becomes more dominant relative to noise, so fewer symbols are detected in error. Accurate DoA estimation consistently outperforms imperfect estimation because the beam remains more precisely aligned with the desired signal, with all curves converging toward very low BER at high SNR (Fig. 6). Growing the array from 12 to 16 elements gives a further, smaller improvement from the extra array gain, indicating that beyond a certain array size the dominant lever for link-level performance is DoA-tracking accuracy rather than raw element count.

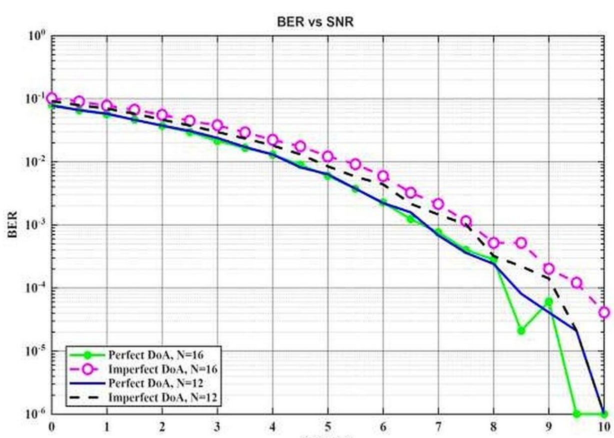

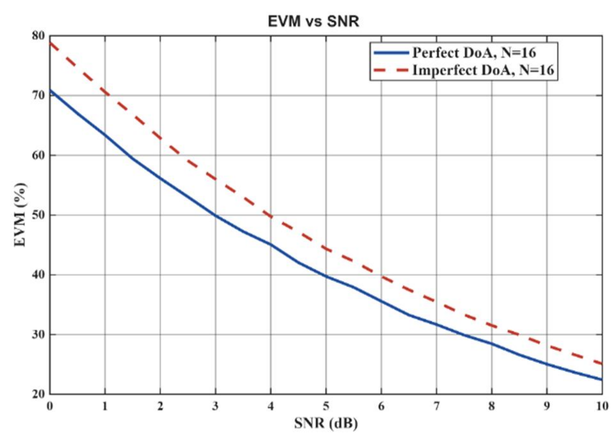

Fig. 6. Bit error rate versus SNR for perfect and imperfect DoA estimation, 12- and 16-element arrays (left). Fig. 7. Error Vector Magnitude versus SNR for the 16-element array, perfect and imperfect DoA estimation (right).

C. Hardware Cost and Power Efficiency

On an illustrative, order-of-magnitude cost scale normalised so a fully phase-shifter-based phased array represents 100% cost (Fig. 8), the conventional (untapered) TMA sits at roughly 35% and the tapered TMA at roughly 45%, reflecting the modest extra complexity of amplitude-weighted switching over simple binary switching, while both TMA variants remain substantially cheaper than a full phase-shifter network. These percentages represent a relative comparison for qualitative evaluation rather than measured implementation costs, and are used consistently in this way wherever they appear in the paper.

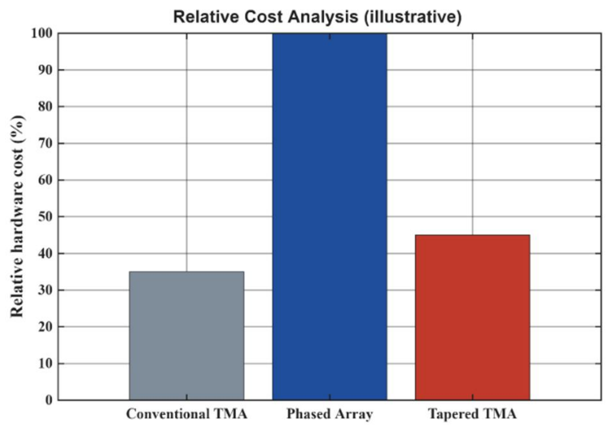

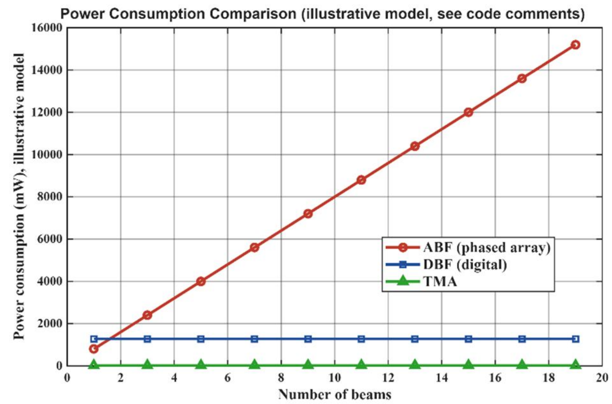

Fig. 8. Illustrative relative hardware cost comparison, normalised to a phase-shifter-based phased array (left). Fig. 9. Illustrative power-consumption model versus number of simultaneous beams for analogue, digital, and tri-state TMA beamforming (right).

D. Multibeam Capability via Harmonic Diversity

Because the tri-state harmonic coefficients of (7) are non-zero for multiple harmonic orders, a shared-aperture two-beam pattern can be synthesised directly from the ±1 harmonic pair, with beams placed at −30° and +30° and sidelobes remaining below about −13 dB in the untapered case (Fig. 10).

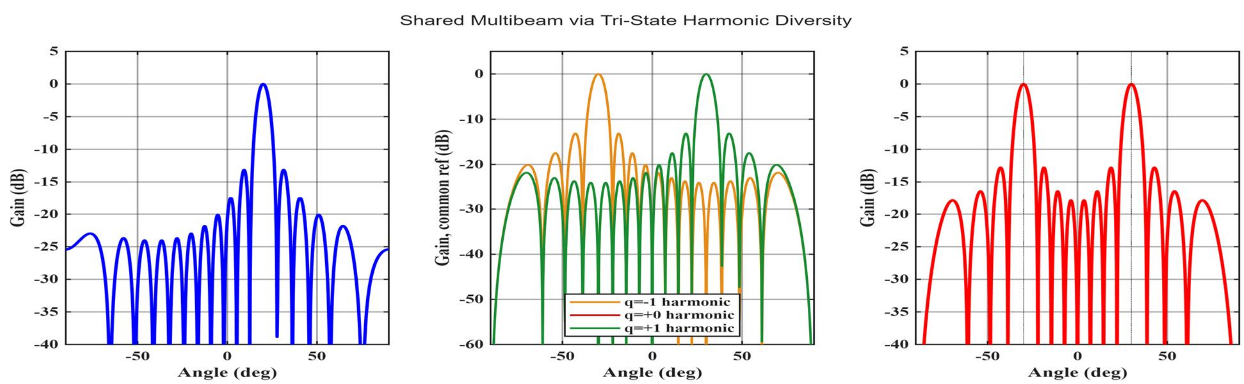

Fig. 10. Shared-aperture two-beam pattern synthesised from the ±1 harmonic pair (beams at −30° and +30°).

A duty-ratio sweep (Fig. 11) shows the ±1 harmonic pair dominating at 0 dB, the ±3 pair sitting roughly 10 dB below, and the ±5 and ±7 pairs staying below −14 dB near α ≈ 1/N. Increasing α narrows the gap between harmonics to within 4–5 dB of the peak — widening how many harmonics could realistically be used for simultaneous, independent beams from a single aperture without additional RF chains, at some cost to per-beam sidelobe control that would need re-optimisation for a multi-user deployment.

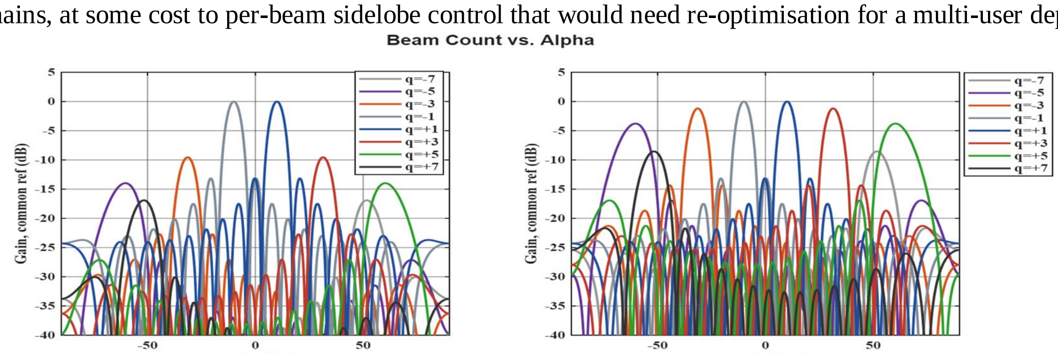

Fig. 11. Effect of modulation duty ratio on harmonic beam distribution, showing the beam-count/sidelobe trade-off across harmonic orders q.

E. Summary Comparison: Binary vs. Proposed Tri-State TMA

Table V summarises the overall improvements achieved by the presented tri-state TMA over the conventional binary TMA. It condenses the results above into a single binary-vs-tri-state comparison, isolating the practical improvement the tri-state + QPO design offers over a conventional binary TMA of the same array size.

Table V. Binary TMA vs. Proposed Tri-State TMA

Parameter	Binary TMA	Proposed Tri-State
SLL	≈ −13 dB	≈ −25.5 dB
HPBW	≈ 6.8°	≈ 8.0°
Gain	≈ 13.6 dBi	≈ 13.3 dBi
SINR (6-interferer)	≈ 8–14 dB	≈ 22 dB
BER at matched SNR	Higher	Lower (near ideal-DoA curve)
Rel. HW cost / power	≈ 35% of phased array	≈ 45% of phased array

Overall, the presented tri-state TMA consistently outperformed the conventional binary TMA across antenna performance, communication quality, and implementation-complexity metrics.

F. Discussion and Limitations

The results indicate that the practical bottleneck for a tri-state TMA is not the switching architecture itself but the choice of switching parameters: uniform duty cycles leave roughly 12 dB of sidelobe suppression on the table relative to the QPO-optimised design, while steering direction and mainlobe width remain essentially unaffected by binary versus tri-state excitation matching the literature's characterisation of TMAs as sidelobe- and harmonic-limited rather than steering-limited.

The present work is simulation-based. Hardware effects such as RF switch insertion loss, mutual coupling, and clock jitter, along with experimental validation on physical hardware, remain part of future work.

VIII. CONCLUSION AND FUTURE SCOPE

This paper developed a tri-state Time-Modulated Array formulation for 5G NR NTN user terminals, deriving closed-form tri-state harmonic coefficients, combining QPO-based sidelobe/beamwidth optimisation with Chebyshev-tapering warm starts, and implementing an ADMM-based Bartlett DoA tracker.

Simulated on a 16-element ULA driven by a realistic 5G NR OFDM waveform, the resulting design pushed SLL from about −13 dB to about −26 dB past the 3GPP-consistent −25 dB target at a gain cost of only around 0.3 dB, while SINR improved by more than 4 dB and DoA tracking remained closely aligned with the ideal case. Together with a cost/power advantage over conventional phased-array and digital beamforming that widens as more beams are required, these results support tri-state TMA beamforming as a workable, lower-complexity, lower-power alternative to phased arrays for NTN terminals.

Future work will target real-time adaptive switching-parameter tuning, evaluation under realistic channel impairments (atmospheric attenuation, Doppler shift, RF switch loss, mutual coupling), and multi-user harmonic-diversity multibeam scaling for 6G/ISAC deployments.

More broadly, the results support the view that the sidelobe and harmonic-utilisation limits historically associated with time-modulated arrays stem from under-parameterised switching control rather than the switching principle itself: given enough degrees of freedom a third excitation state, an independently placed negative pulse, and a jointly solved SLL/HPBW objective a TMA can approach phased-array-like pattern quality while retaining switch-based hardware's cost and power advantage.

REFERENCES

[1] G. G. Lema, E. Lagunas, M. R. Bhavani Shankar, and J. Grotz, "Time Modulated Arrays Beamforming for Non-Terrestrial Network User Terminal," IEEE Open Journal of the Communications Society, vol. 6, pp. 271–288, 2025.
[2] W. H. Kummer, A. Villeneuve, T. S. Fong, and F. G. Terrio, "Ultra-Low Sidelobes from Time-Modulated Arrays," IEEE Transactions on Antennas and Propagation, vol. 11, no. 6, pp. 633–639, 1963.
[3] C. A. Balanis, Antenna Theory: Analysis and Design, 4th ed. Hoboken, NJ, USA: John Wiley & Sons, 2016.
[4] H. L. Van Trees, Optimum Array Processing, Part IV of Detection, Estimation, and Modulation Theory. New York, NY, USA: Wiley, 2002.

[5] S. Boyd, N. Parikh, E. Chu, B. Peleato, and J. Eckstein, "Distributed Optimization and Statistical Learning via the Alternating Direction Method of Multipliers," Foundations and Trends in Machine Learning, vol. 3, no. 1, pp. 1–122, 2011.
[6] 3GPP TS 38.211, NR; Physical Channels and Modulation, Release 17, 2023.
[7] 3GPP TS 38.300, NR; Overall Description; Stage-2, Release 17, 2023.
[8] M. M. Azari et al., "Evolution of Non-Terrestrial Networks From 5G to 6G: A Survey," IEEE Communications Surveys & Tutorials, vol. 24, no. 4, pp. 2633–2672, 2022.

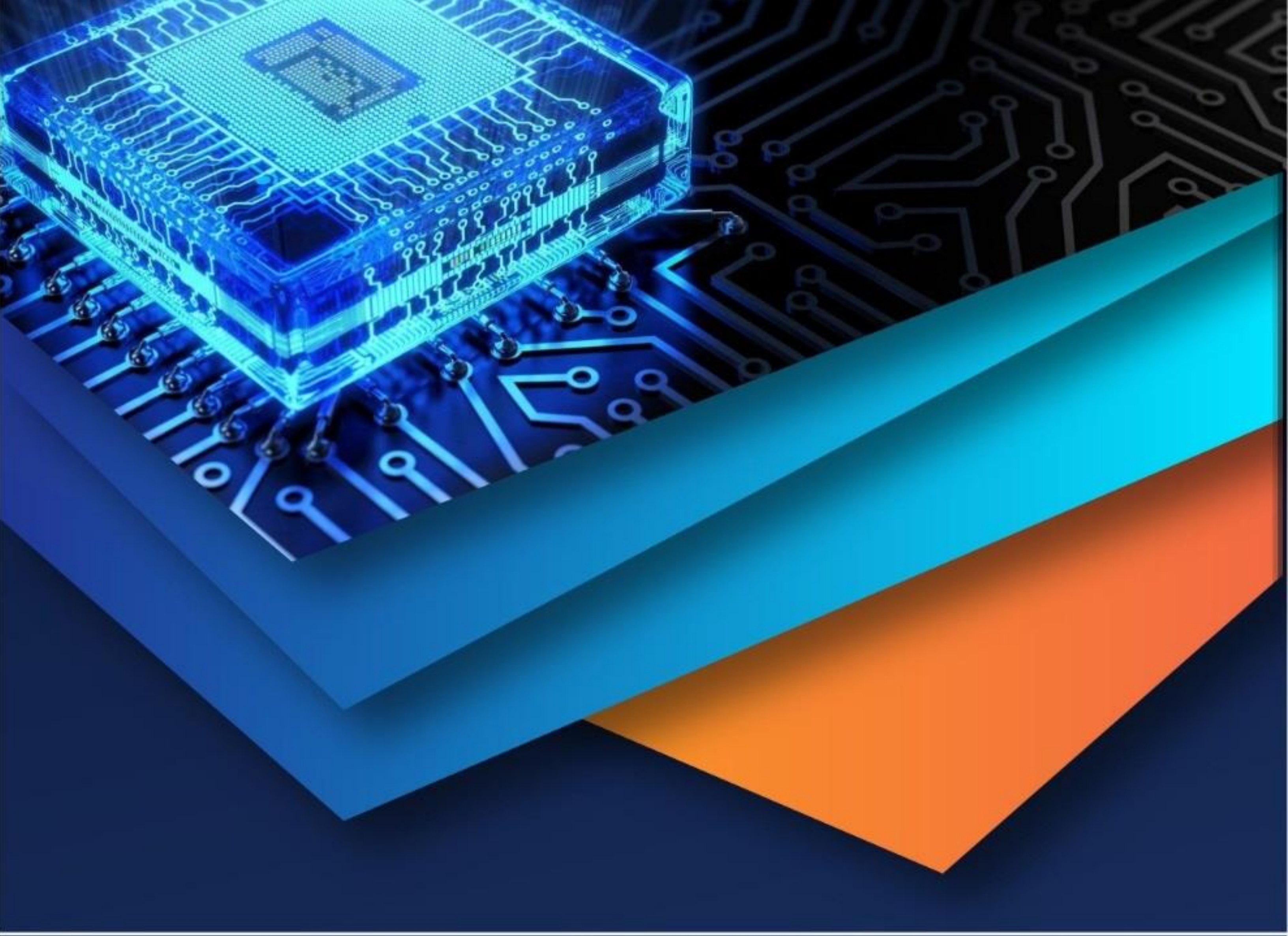

10.22214/IJRASET

INDEX COPERNICUS 45.98

IMPACT FACTOR: 7.129

IMPACT FACTOR: 7.429

INTERNATIONAL JOURNAL FOR RESEARCH

IN APPLIED SCIENCE & ENGINEERING TECHNOLOGY